



Estimation of interbasin transport using ocean bottom pressure: Theory and model for Asian marginal seas

Y. Tony Song¹

Received 28 July 2005; revised 30 January 2006; accepted 1 August 2006; published 3 November 2006.

[1] The Asian Marginal Seas are interconnected by a number of narrow straits, such as the Makassar Strait connecting the Pacific Ocean with the Indian Ocean, the Luzon Strait connecting the South China Sea with the Pacific Ocean, and the Korea/Tsushima Strait connecting the East China Sea with the Japan/East Sea. Here we propose a method, the combination of the “geostrophic control” formula of Garrett and Toulany (1982) and the “hydraulic control” theory of Whitehead et al. (1974), allowing the use of satellite-observed sea-surface-height (SSH) and ocean-bottom-pressure (OBP) data for estimating interbasin transport. The new method also allows separating the interbasin transport into surface and bottom fluxes that play an important role in maintaining the mass balance of the regional oceans. Comparison with model results demonstrates that the combined method can estimate the seasonal variability of the strait transports and is significantly better than the method of using SSH or OBP alone.

Citation: Song, Y. T. (2006), Estimation of interbasin transport using ocean bottom pressure: Theory and model for Asian marginal seas, *J. Geophys. Res.*, *111*, C11S19, doi:10.1029/2005JC003189.

1. Introduction

[2] Exchanges of water mass often happen between two basins interconnected by a shallow strait or a deep sill, since an imbalanced pressure gradient between the two basins can be formed through a number of physical processes, such as wind forcing, inflow from an adjacent basin, seasonal evaporation, or surface cooling in high latitudes. The pressure gradient force within the water column between the two interconnected basins can drive the water above sill depth out through the passage into another basin. For example, *Wyrki* [1987] has noticed that the pressure difference from the Pacific to the Indian Ocean is the main driving force behind the annual variability of the Indonesian Throughflow. The transport in a strait can be a unidirectional or critically controlled bidirectional flow, depending on the geometry of the strait and the source of the bottom water [Whitehead et al., 1974; Killworth, 1995; Pratt, 2004]. When the outflow rate equals the accumulation rate of water mass or bottom pressure, the interface ceases to rise and a steady state is achieved. Volume fluxes of such outflows are useful measurements of interbasin water exchange, which are of fundamental interest to physical oceanography [Whitehead, 1989, 1998; Godfrey, 1996; Susanto et al., 2000; Susanto and Gordon, 2005] and ocean climate considerations [Dickson et al., 1999; Hansen et al., 2001; Gordon et al., 2003].

[3] However, interbasin transport is difficult to measure [Hansen et al., 2001; Gordon and Fine, 1996; Susanto and

Gordon, 2005] because of the geographical complexity associated with interconnected basins. The Asian marginal seas are one of these examples, as shown in Figures 1 and 2, which have a highly complex geometry because they interconnect through a number of narrow straits and sills. These marginal seas include the South and East China Seas (SCS and ECS), Japan/East Sea, Sulu Sea, Celebes Sea, and the Philippine Sea, which are interconnected by the Luzon Strait, Taiwan Strait, Makassar Strait, and the Sibutu Passage. This combination of geometry, connectivity with the Pacific and Indian Oceans, and seasonally reversing monsoon winds contributes to one of the most complicated current systems in the world oceans [Metzger and Hurlburt, 1996; Hu et al., 2000; Song and Tang, 2002]. As the most energetic western boundary current of the Pacific, the Kuroshio is particularly difficult to measure with conventional instruments [Li et al., 1998] and simulate with a numerical ocean model [Hsueh et al., 1997] due to its different processes and the wide range of time and length scales associated with its dynamics. The circulation patterns and interbasin exchanges of water masses in the region have been of great interest because of their effects on the El Niño-Southern Oscillation (ENSO) development [Godfrey, 1996; Qu et al., 2004, 2005]. Despite many previous studies [Shaw, 1991; Wajsowicz, 1993; Metzger and Hurlburt, 1996; Qu et al., 2000, 2006], it is still challenging to obtain sufficient in-situ data and accurate models for a full understanding of the interbasin transports and their role in the general circulation of the ocean.

[4] In this study, we have extended the existing hydraulic control theory of Whitehead et al. [1974] allowing the use of ocean bottom pressure (OBP), which will be available from the U.S.-German Gravity Recovery and Climate Experiment (GRACE) mission [Tapley et al., 2004]. The

¹Jet Propulsion Laboratory, California Institute of Technology, Pasadena, California, USA.

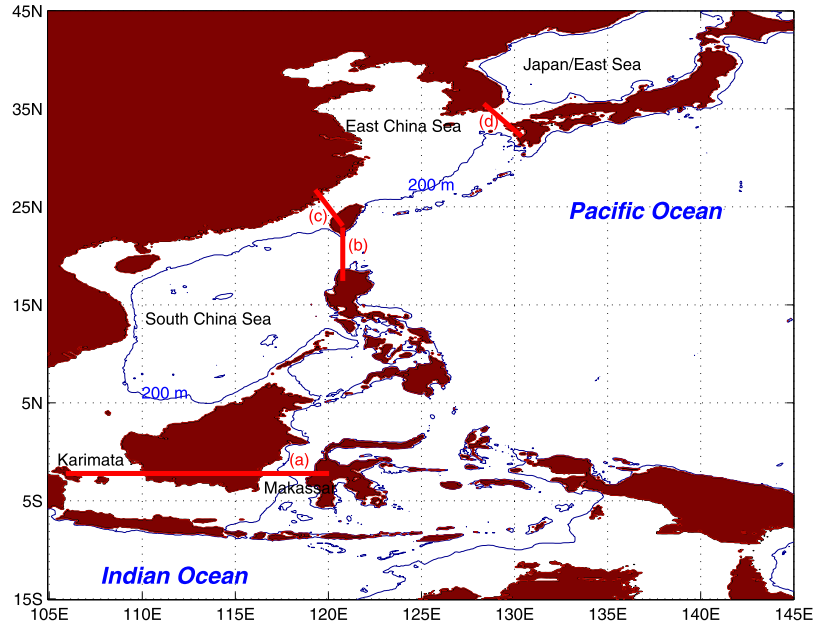


Figure 1. Geographic location of the four Straits: (a) Karimata-Makassar Strait at 3°S; (b) The Luzon Strait from Phillipinne to Taiwan at 121°E; (c) Taiwan Strait from Taiwan to the main land at about 120°E; and (d) The Korea/Tsushima Strait at about 131°E.

method also combines the “geostrophic control” formula of *Garrett and Toulany* [1982] allowing the use of sea-surface-height (SSH). Their combination produces a simple and inexpensive estimate of fluxes for interbasin exchanges of water mass. A non-Boussinesq ocean model [Song and Hou, 2006] properly designed to simulate GRACE-proxy OBP and SSH will be used to test the proposed method.

2. Theory of Rotating Hydraulic Control

[5] According to the theory of rotating hydraulics [Whitehead *et al.*, 1974; Whitehead, 1989, 1998], the cross-sill exchange of water mass in the bottom layer is largely governed by the following fundamental principles: inertia, rotation, and pressure gradient. This theory can be illustrated by the “reduced gravity” equations for flow in the bottom layer:

$$V_b \bullet \nabla V_b + f \times V_b = -g' \nabla h \quad (1)$$

Here $V_b = (u_b, v_b)$ is the two-dimensional horizontal flow in the bottom layer, f is the Coriolis parameter, $g' = g\delta\rho/\rho$ is the reduced gravity, ρ is density, g is the gravity coefficient, δ is the vertical difference operator, ∇ is the horizontal gradient operator, and h is the layer interface depth, as shown in Figure 3. The first term of the equation represents the transport of momentum by the fluid, corresponding to the force due to the inertia of the fluid as the fluid moves from place to place. The second term is the Coriolis force due to the Earth’s rotation. The third term in the right-hand-side of the equation is the pressure gradient force. *Whitehead* [1989] examined the balance of the three terms: (1) balancing the Coriolis force with the pressure gradient force gives the geostrophic relation, i.e., $fv_b = g'h_x$, where v_b is the flow component along the strait and h_x is the gradient across the strait; (2) taking the curl of the above equation and using

continuity gives the conservation of potential vorticity, i.e., $v_{bx} - u_{by} + f = q(\psi)h$, where $q(\psi)$ is the potential vorticity and ψ is the streamfunction; (3) integrating along streamlines yields Bernoulli’s law in the form:

$$\frac{v_b^2}{2} + g'h = B(\psi). \quad (2)$$

Berloully’s law is simply an expression of converting the difference of potential energy between the two basins into kinetic energy. Based on the above relations, several simple formulas have been derived to estimate the mean flows in deep straits. *Whitehead et al.* [1974] and *Whitehead* [1989] give the following formulation:

$$Q = \begin{cases} \frac{g'h_u^2}{2f} & \text{if } R = \frac{\sqrt{2g'h_u}}{f} < W \\ \left(\frac{2}{3}\right)^{3/2} W \sqrt{g'} \left[h_u - \frac{f^2 W^2}{8g'}\right]^{3/2} & \text{otherwise.} \end{cases} \quad (3)$$

Here W is the width of the strait, h_u is the height of the interface over the sill, and R is the Rossby radius of deformation. *Whitehead* [1989] has been successfully applying the formulation to estimate the mean transport for a number of overflow cases, such as the Denmark Strait, the Iceland-Faeroe sill, and the Vema Channel. However, the hydraulic theory is limited to only bottom-layer flows and has not been extended to general applications because the density profiles of $\delta\rho = \rho_B - \rho_A$, one on each side of the sill, in seasonal or interannual scales, are difficult to obtain [Qu *et al.*, 2006].

3. Two-Layer Theory of Ocean Bottom Pressure

[6] In oceanic studies, less attention has been given to ocean bottom pressure (OBP), the counterpart of the atmo-

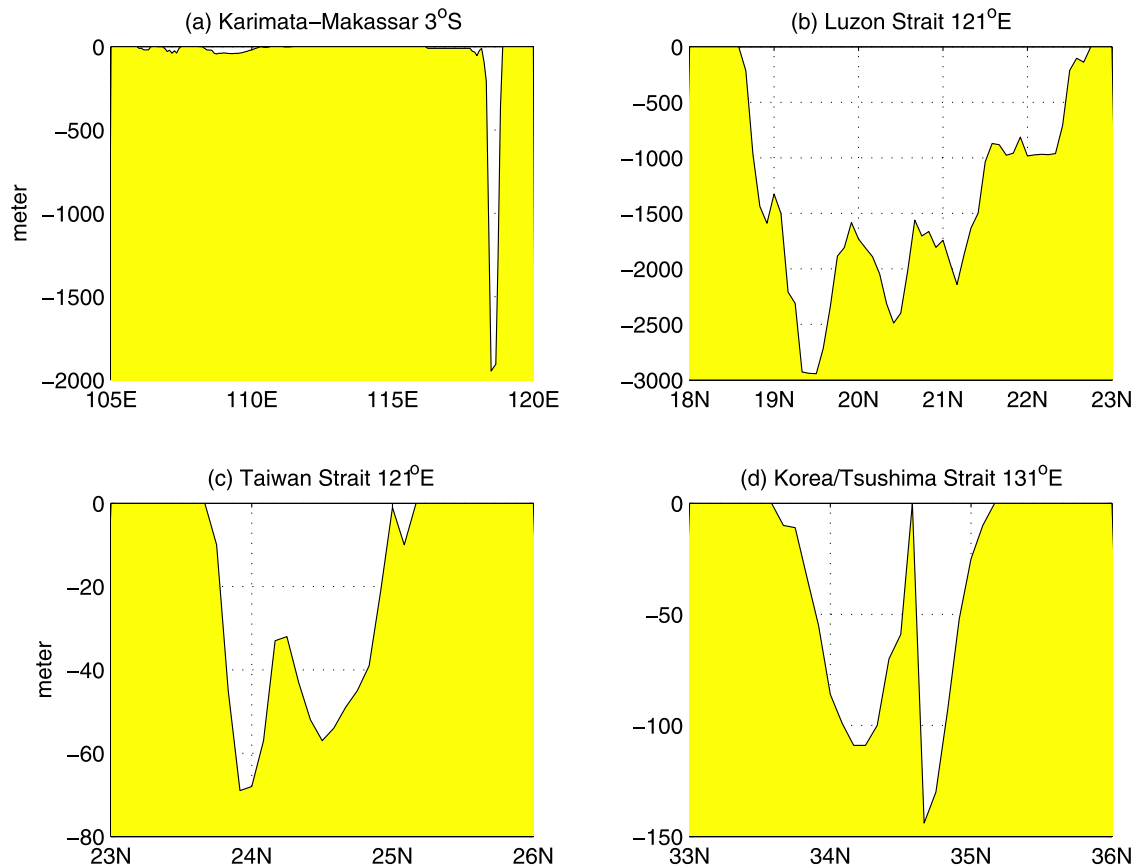


Figure 2. Cross sections of these four straits, as marked by the red bars in Figure 1, respectively.

spheric surface pressure, because pressure at the ocean bottom is difficult to measure. So far, only a few local measurements over a short time period have been available [e.g., Luther *et al.*, 1990; Hughes and Smithson, 1996]. In fact, OBP is the vertical integral of water mass; therefore, it contains information on atmospheric pressure and the oceanic response to it, plus ocean dynamics and the oceanic forces acting on the topography [Wahr *et al.*, 1998; Song and Zlotnicki, 2004].

[7] The lack of ocean bottom pressure data has changed after the launch of the U.S.-German Gravity Recovery and Climate Experiment (GRACE) satellites, which provide monthly estimates of the Earth’s gravity field on spatial scales of a few hundred kilometers [Wahr *et al.*, 2004]. On these timescales, changes in the gravity field can be interpreted as changes in a thin layer of water covering the Earth, which, over the oceans, is equivalent to ocean bottom pressure [Hughes *et al.*, 2000]. The design accuracy of GRACE is equivalent to a surface mass density of a few millimeters at those spatial scales and longer [Wahr *et al.*, 1998], although in the first data release, the actual accuracy is closer to 1.5 cm [Wahr *et al.*, 2004]. So far, 22 months of GRACE data has been released. Initial analysis of the data has shown strong OBP signals in high latitudes [Zlotnicki *et al.*, 2006]. In addition, the European Space Agency (ESA) has planned to launch the Gravity Field and Stead-state Ocean Circulation Explorer (GOCE) in 2006 [Drinkwater *et al.*, 2003]. These satellite observations will provide unprecedented global resolution and accuracy of OBP data, which

may revive interest among oceanographers. In addition, the GRACE-derived OBP complements the existing TOPEX/Poseidon-Jason-observed SSH. In a homogeneous hydrostatic ocean, sea surface and bottom pressure variations are identical. In a stratified ocean, however, the two can be very different. The combination of GRACE data, representing oceanic mass changes, and TOPEX/Poseidon-Jason

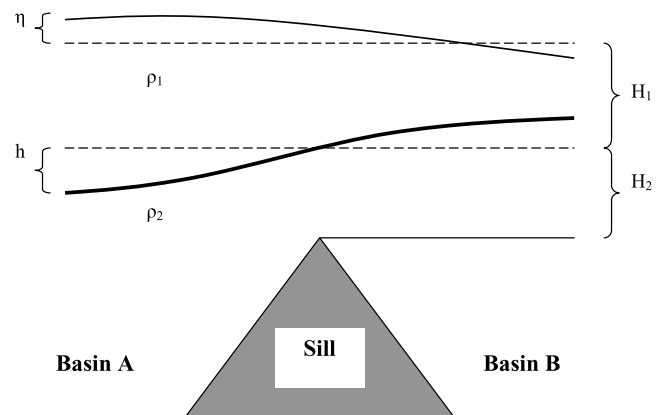


Figure 3. Vertical view of the two-layer flow along the sill that separates the two basins. H_1 is the thickness of the upper layer with density ρ_1 and H_2 is the thickness of the lower layer with density ρ_2 . η and h are the anomaly from the mean sea-surface-height and layer interface, respectively.

data, representing ocean volume changes, is very powerful [Jayne *et al.*, 2003; Song and Zlotnicki, 2004].

[8] To give a theoretical explanation for using OBP in estimating the interbasin transport of water mass, let us consider a simple two-layer ocean, as shown in Figure 3. The total OBP at the depth level of sill tip can be written as:

$$P_b = g\rho_1(\eta + H_1 - h) + g\rho_2(H_2 + h). \quad (4)$$

Here H_1 and H_2 are the steady-state layer thickness; η and h are their anomaly; and ρ_1 and ρ_2 are the density of the two layers, respectively. The pressure difference across the sill that separates the two basins is:

$$\Delta P_b = P_b^B - P_b^A = g\rho_1\Delta\eta + g(\rho_2 - \rho_1)\Delta h, \quad (5)$$

where $\Delta\eta$ is the SSH difference across the sill and Δh is the layer-interface difference across the sill. It can be seen that the pressure difference is the combination of the SSH and layer-interface differences between the two basins. As SSH can be obtained from satellite altimeters such as the TOPEX and Jason-1, the GRACE-derived OBP is the only variable needed to determine the interface changes of the idealized two-layer ocean. This two-layer model provides the theoretical framework for using satellite-observed SSH and OBP to estimate interbasin exchanges of water mass.

[9] For convenience, OBP often refers to the normalized bottom pressure as the thickness of water mass, i.e., the normalized dynamic height (i.e., $p_b = \int_{-H}^{\eta} g\rho dz / g\rho_0 = P_b / g\rho_0$). In this way, the OBP would have the same dimension as the SSH in meters. Without particular indication, hereafter, we will refer the OBP as the normalized dynamic height (equivalent to the thickness of water). The cross-sill bottom pressure difference can be written as

$$\Delta p_b = \frac{\rho_1}{\rho_0}\Delta\eta + \frac{\rho_2 - \rho_1}{\rho_0}\Delta h. \quad (6)$$

It can be seen that the interface difference Δh can be determined by the differences of SSH and OBP in the form:

$$g'\Delta h = g(\Delta p_b - \Delta\eta), \quad (7)$$

with assumption of $\rho_1 \approx \rho_0$. Based on the two-layer theory, we use the ‘‘geostrophic control’’ formula of Garrett and Toulany [1982] for the upper layer and the ‘‘hydraulic control’’ formulation of Whitehead *et al.* [1974] for the lower layer (as derived mathematically in Appendix A), then combine them together allowing using OBP and SSH to estimate the strait transport:

$$Q = \begin{cases} \frac{g}{f} \left\{ H_1\Delta\eta + \frac{H_2}{2}(\Delta p_b - \Delta\eta) \right\} & \text{for } R < W \\ \frac{g}{f} H_1\Delta\eta + \kappa \left(\frac{2}{3} \right)^{3/2} H_2 W \sqrt{g|\Delta p_b - \Delta\eta|} & \text{otherwise} \end{cases}. \quad (8)$$

Here H_1 and H_2 are the surface and bottom layer depth, W is the strait width, $R = \sqrt{2g'\Delta h/f}$ is the mean Rossby radius of deformation, $\kappa = \text{sign}(\Delta p_b - \Delta\eta)$ determines the gradient direction, and $\Delta\eta$ and Δp_b are the SSH and OBP difference

from the up-stream basin to the down-stream basin, respectively. The new formulation has two important features: First, the OBP anomaly Δp_b is measurable from satellite, thus providing spatial and temporal continuous data that can be used to estimate both long- and short-term variability of the transport. Second, because the SSH is also available from satellite, the formulation can be used to separate the surface-layer transport from the bottom-layer transport and to characterize the flow that is governing the water mass in the two adjacent basins.

[10] However, it should be noted that the change of water mass far below the sill depth may also affect the pressure difference and would not necessarily contribute to the force that drives the overflow. Fortunately, deep water formation is a much slower process than the problems we are interested in here. For the time-scales of annual and shorter, the contribution from the deep water formation is quite small and may not affect our estimation significantly.

4. Model Verification

[11] In this section, we focus on verifying the derived theoretical formulation. Ideally, we like to use in-situ measurements and GRACE-derived OBP data for the verification. Unfortunately, long-term datasets are not available (several efforts are underway to obtain the data [e.g., Zlotnicki *et al.*, 2006]) at this time. As the first step of the study, we have used model-generated GRACE-proxy data for the verification.

[12] Our model is based on the non-Boussinesq parametric vertical coordinate model of Song and Hou [2006], which allows multiscale applications with both Boussinesq and non-Boussinesq conditions. The non-Boussinesq approximation, when applied to ocean models, implies that seawater is compressible, so that mass, rather than volume, is conserved. Therefore, the OBP can be directly calculated based on conservation of mass, and the sea surface elevation η can be retrieved from the pressure values by:

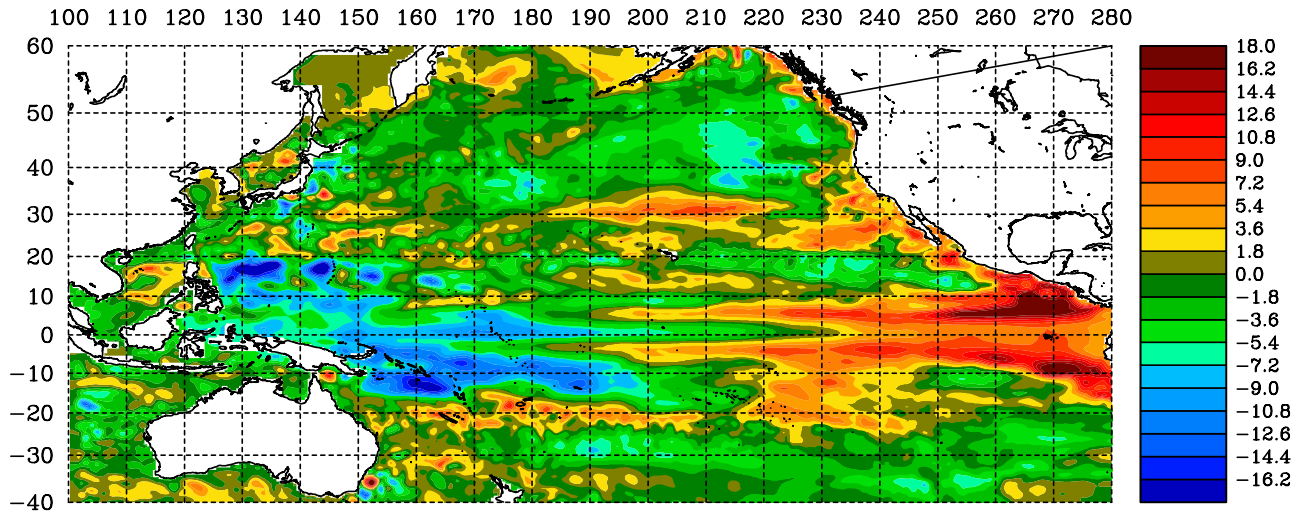
$$\eta = \int_{-1}^0 \delta p / (g\rho) ds - H, \quad (9)$$

where H is the bottom topography, ρ is the density within the pressure layer δp , and s is the parametric vertical coordinate system [Song and Haidvogel, 1994] (Y. T. Song *et al.*, A non-Boussinesq terrain-following ocean general circulation model for GRACE applications, submitted to *Advances in Geosciences*, 2006, hereinafter referred to as Song *et al.*, submitted manuscript, 2006). In the above formulation, the sea surface elevation is obtained while considering the heat expansion/contraction of the seawater. The mass-conserving model is important for separating the contributions from SSH in the total pressure gradient force. For example, a motionless ocean that is uniformly heated at the surface will not experience sea level change. As Huang and Jin [2002] points out, the conventional Boussinesq approximations might ignore the heat expansion/contraction physics that represent the real ocean and are inconsistent with either T/P or GRACE data.

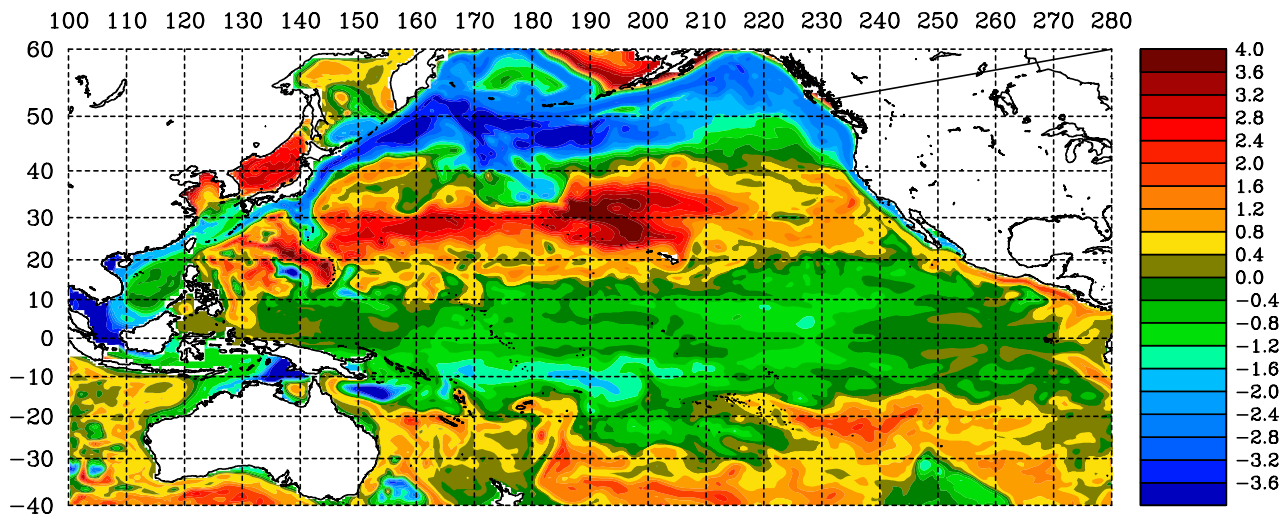
[13] Based on the new model formulation, a non-Boussinesq global ocean model (Song *et al.*, submitted manuscript, 2006) has been developed on JPL’s parallel

Pacific Ocean 0.5x0.5 Grid (NB & Yearly-mean removed)

18045.03 Day : 15 Feb 1998 - 00: 47



a) SSH Anomaly (cm)



b) OBP Anomaly (mb)

Figure 4. Model results: (a) sea-surface-height (SSH) anomaly, representing volume change; (b) ocean-bottom-pressure (OBP) anomaly, representing mass change. Note the bottom pressure anomaly is normalized by $(P_b - P_b^0)/g\rho_0$, where P_b is the bottom pressure and P_b^0 is the time-mean bottom pressure. Units are cm for SSH and mbar for OBP.

computer. The global model has a grid resolution of $0.5^\circ \times 0.5^\circ$ with enhanced resolution to $1/3^\circ$ in the tropical region from 30°S to 30°N , covering the world's oceans from 75°S to 75°N . The bottom topography is from ETOPO5, with a minimum depth of 20 m near the coastal wall and a maximum depth of 5500 m in the deep ocean. The water depth is divided into 20 topography-following levels. The model starts with the initial conditions of annual mean temperature and salinity from Levitus. The surface forcing are monthly mean air-sea fluxes of momentum, heat, and freshwater from NCEP/NCAR reanalysis data. For the heat and salt flux, a thermal feedback term is applied. The

model is first spun-up to 50 years with the annual-mean forcing, and then integrated from year 1948 to year 2003 by the monthly-mean forcing. Figure 4 displays the model SSH and OBP, the GRACE-proxy data generated by the non-Boussinesq ocean model for the Pacific Ocean. The SSH anomaly in February 1998 (top panel) has a positive anomaly in the eastern equatorial Pacific, indicating the peak of the ENSO event of 1997 and 1998. The OBP (bottom panel) shows a corresponding positive anomaly in the eastern equatorial Pacific, but the most significant feature is the huge mass shift from higher latitudes ($30 \sim 60^\circ\text{N}$) to lower latitudes ($10 \sim 30^\circ\text{N}$). The reason for such a huge mass

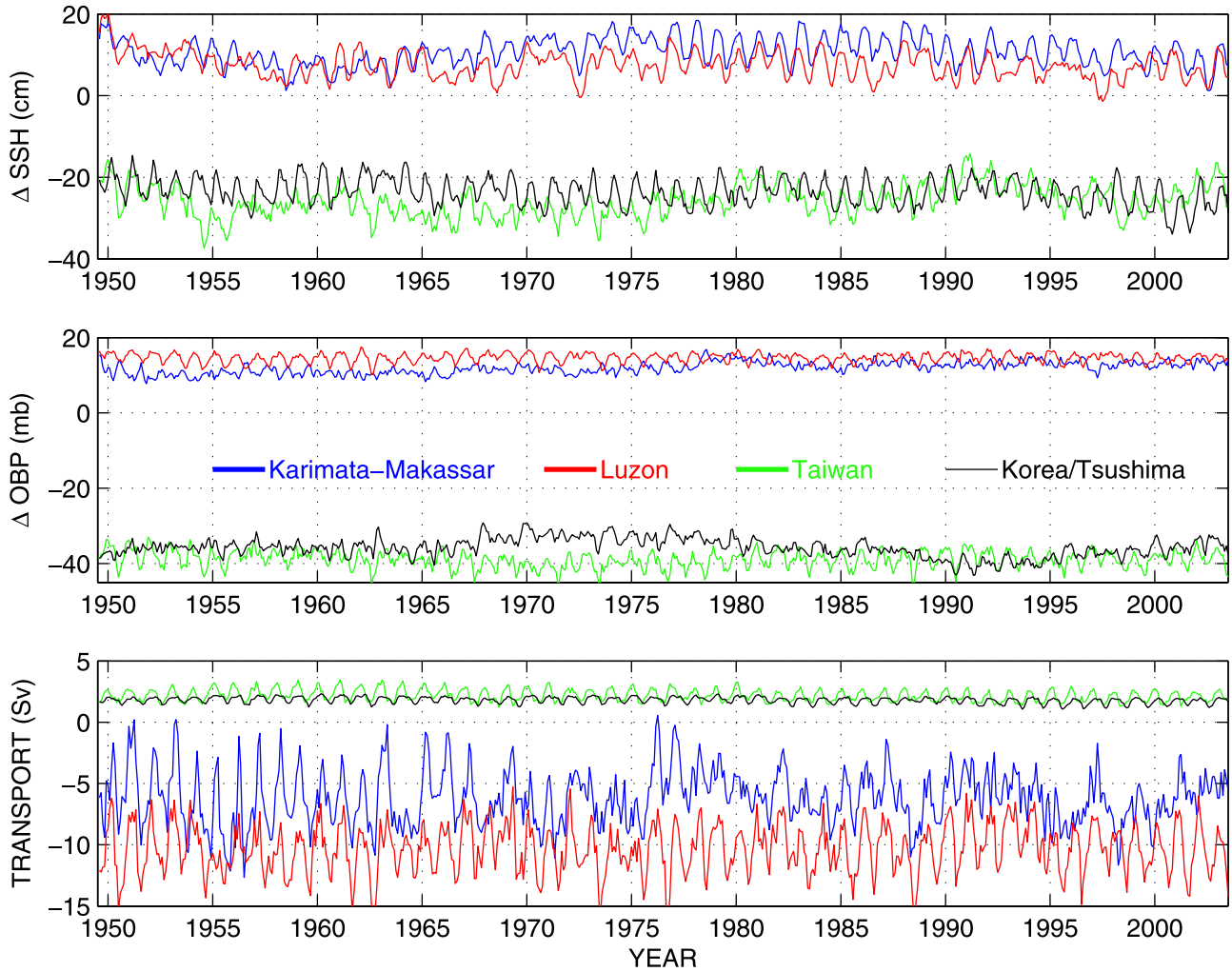


Figure 5. Time series of SSH difference (top), OBP difference (middle), and corresponding cross-strait transports (bottom) between two interconnected basins. The interbasin differences are calculated in the following way: The Karimata-Makassar difference (blue) is the SCS and the western Pacific [105°E ~ 140°E, Eq ~ 24°N] minus the eastern Indian Ocean [105°E ~ 130°E, 20°S ~ 10°S]; The Luzon difference (red) is the western Pacific [122°E ~ 140°E, Eq ~ 30°N] minus the SCS [105°E ~ 120°E, Eq ~ 24°N]; The Taiwan difference (green) is the ECS [121°E ~ 126°E, 28°N ~ 40°N] minus the SCS [105°E ~ 120°E, Eq ~ 20°N]; The Korea/Tsushima difference (black) is the Sea of Japan [130°E ~ 140°E, 34°N ~ 48°N] minus the ECS [121°E ~ 126°E, 28°N ~ 40°N]. The Indonesian Strait and Luzon Strait transports (blue and red) are southward and westward, respectively. The Taiwan Strait and Korea/Tsushima Strait transports (green and black) are northeastward.

redistribution is unclear in the SSH data alone, indicating that the bottom pressure provides additional information which cannot be seen in the surface. The model results have been compared with GRACE data by *Zlotnicki et al.* [2006].

[14] It should be noted that GRACE only gives OBP anomaly, not the absolute value of the pressure; therefore, it cannot be used to obtain the mean transport. To resolve this problem, we propose to decompose the total transport into three components: mean transport, annual cycle, and inter-annual variability (residual), i.e.,

$$Q(t) = Q_{\text{mean}} + Q_{\text{annual}}(t) + Q_{\text{residual}}(t) \quad (10)$$

In the following, we will consider the three components separately. Specifically, the mean transport can be estimated by the original hydraulic control approach of *Whitehead*

[1989], which will not be discussed here. The annual cycle and interannual variability will be obtained from SSH and OBP data. Figure 5 gives the differences of SSH and OBP between two inter-connected basins and their corresponding transports from the model. Before using the model to verify our theoretical formulation, we first compare the model results with known observations:

[15] 1. For the Karimata-Makassar throughflow (blue line), the model gives a mean transport of 7.5 Sv with a maximum of 8.9 Sv in February and a minimum of 5.2 Sv in September. All of them are southward transport from the Pacific Ocean and SCS to the Indian Ocean. Some observational data for the throughflow, although not complete, is available. For example, *Wyrski* [1961] studied the Karimata Strait and gave the southward transport of maximum 4.5 Sv in winter and northward transport of maximum 3.5 Sv in

Table 1. Summary of the Strait Parameters and Their Mean Transports

| Strait | H_1 , m | H_2 , m | W (Lower-Layer), km | f , 10^{-4} s^{-1} | Q_{Model} , Sv | Q_{Obs} , Sv |
|-------------------|-----------|-----------|-----------------------|--------------------------------|------------------|----------------|
| Karimata-Makassar | 400 | 1000 | 15 | -0.25 | 7.5 | 4 ~ 9 |
| Luzon Strait | 1500 | 900 | 27 | 0.55 | 10.2 | 2 ~ 10 |
| Taiwan Strait | 120 | 0 | 48 | 0.59 | 2.2 | ~2 |
| Korea/Tsushima | 120 | 20 | 40 | 0.94 | 2.1 | 2 ~ 3.5 |

summer. Recently, *Susanto and Gordon* [2005] measured the Makassar Strait flow and gave a mean transport of 8 Sv. The combination of the two observations compares favorably with our model results.

[16] 2. For the Luzon Strait (red line), our model gives a mean westward transport of 10.2 Sv with maximum 12.2 Sv in January and a minimum of 8.2 Sv in July. *Metzger and Hurlburt* [1996] estimated that the westward transport is between 0.5 Sv and 8.1 Sv. *Qu et al.* [2004] gave a maximum westward transport of 6.1 Sv in winter and a minimum eastward transport of 0.9 Sv in summer. *Chu and Li* [2000] gave the largest estimate, with a maximum of 13.7 Sv in February and a minimum of 1.4 Sv in September. Again, our model results are consistent with these previous estimations in both amplitude and annual cycle.

[17] 3. For the Taiwan Strait transport (green line), there is less observed data, except *Fang* [1995], who gave an estimate of 2 Sv northeastward transports based on some ADCP measurement that is consistent with our model result of 2.2 Sv.

[18] 4. For the Korea/Tsushima Strait (black line), our model gives a mean northeastward transport of 2.1 Sv with

a maximum of 2.3 Sv in July and a minimum of 1.7 Sv in February. *Kim et al.* [2004] measured the western channel of Korea Strait and gave a mean transport of 1.5 Sv with a maximum of 1.9 Sv in October and a minimum of 1.2 Sv in February. *Fang* [1995] gave an estimate of 2 Sv for the Tsushima current. Adding these two estimates gives the total mean transport of 3.5 Sv for the Korean/Tsushima Strait, which is much higher than our model results.

[19] In summary, the model agrees reasonably well with the observations. The agreement gives confidence in the validity of the model for verifying the proposed theoretical formulation.

[20] Table 1 gives the geometric parameters of the four straits and their mean transports derived from the model and observations. The upper-layer depth of 400 m for the Makassar Strait is based on the work of *Meyers et al.* [1995] and the average width of 15 km for the bottom layer is based on the data of *Susanto and Gordon* [2005]. The upper-layer depth of 1500 m for the Luzon Strait is determined by the bifurcation point of the mean density profiles on both sides of the strait and has been used by *Qu et al.* [2006] for deriving the deep overflow into the South China Sea. Although the deepest

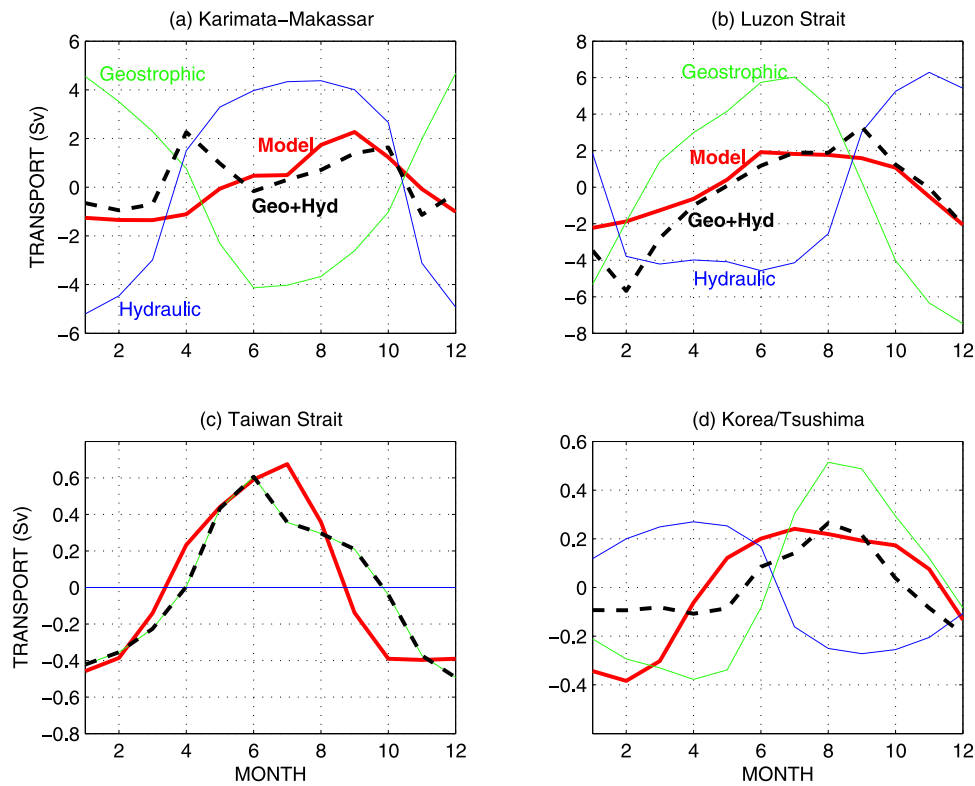


Figure 6. Mean seasonal transports from model (red) and from the theoretical estimation: by SSH-only using the geostrophic control (green) formula, by OBP-only using the hydraulic control theory (blue), and by their combination (dashed). The positive values are northward or eastward transport, while the negative values are southward or westward transport.

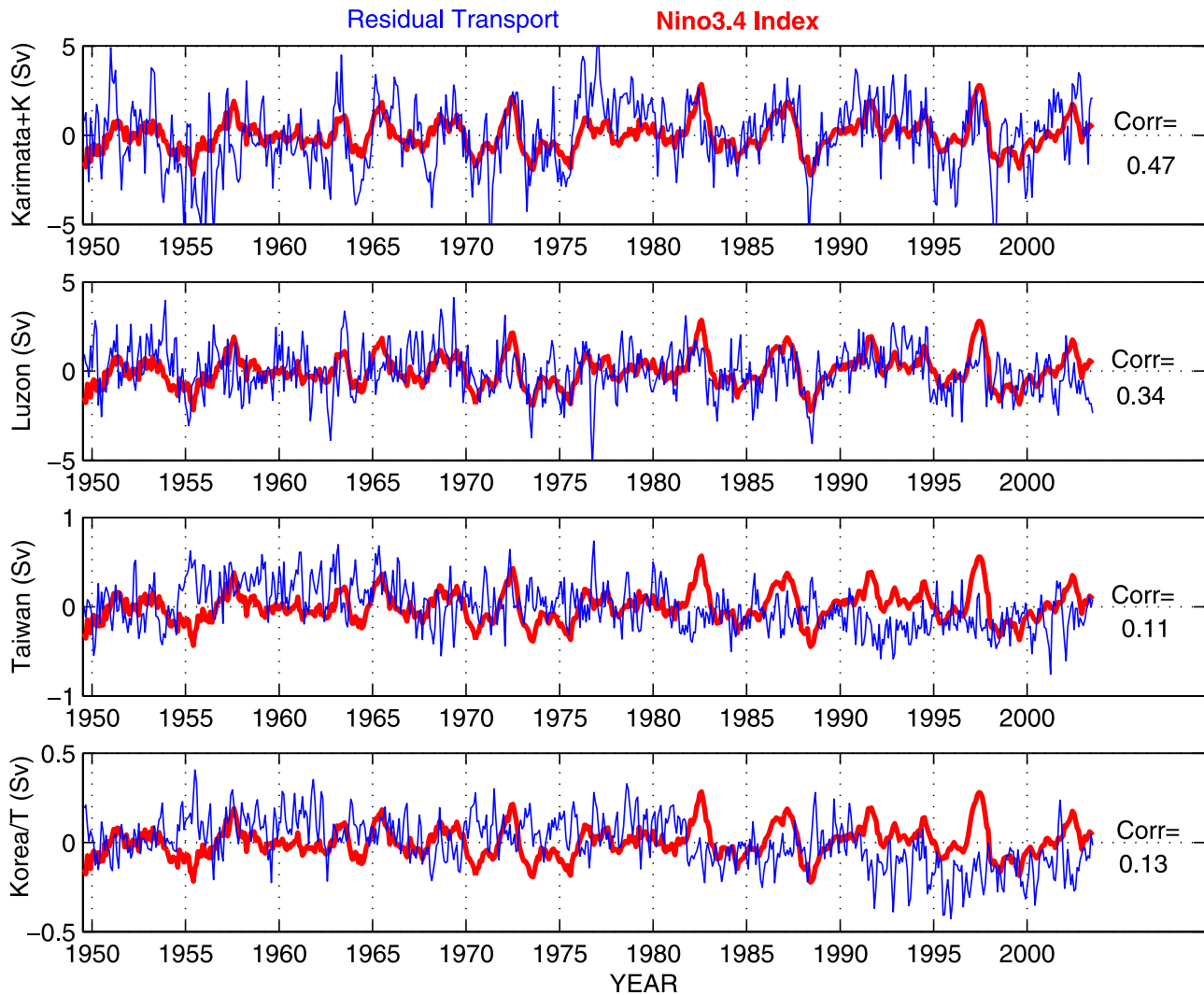


Figure 7. Comparison of the residual transport (after removing the seasonal cycle) with Nino3.4 index (scaled). A long-term trend is also removed. Their correlation coefficient for each strait is shown in the panel. The transports of the Karimata-Makassar and Luzon straits (top two panels) have a stronger correlation with the Nino3.4 Index than those of the Taiwan and Korea/Tsushima straits.

channel is the Bashi Channel with a width of only 17 km, as noticed by *Qu et al.* [2006], we have chosen the averaged channel width of 27 km for the bottom layer because there are other channels below 1500 m (Figure 2). The parameters for the Taiwan Strait and Korea/Tsushima Strait are estimates from the ETOPO5 topographic data.

[21] Here we compare the theoretical estimations (dashed) of the annual cycle with the model results (red) for the four straits, as shown in Figure 6. The annual cycle is averaged over the years 1950 to 2003 after removing the mean value. It can be seen that the theoretical estimations agree well with the model, except for the Korea/Tsushima Strait, in which the theoretical estimation and model has a phase mismatch of about one month. The mismatch is probably due to the island that separates the strait into two channels. In addition, the Karimata-Makassar transport has a big discrepancy with the model in spring. The discrepancy is probably due to the modulated transports within the Indonesian archipelago, which cannot be represented by the simple theoretical formulation. To separate the

volume transport into surface and bottom fluxes, we also calculate the surface-layer transport (green) using SSH data by the “geostrophic control” formula and the bottom-layer transport (blue) using SSH and OBP data by the “hydraulic control” formulation. First, it can be seen that the surface-layer flux (green curve) and bottom-layer flux (blue curve) of the Karimata-Makassar Strait, Luzon Strait, and Korea/Tsushima Strait have opposite signs of annual cycle, indicating that the bottom-layer transport compensates for the surface-layer transport in the total transport. Second, the Taiwan Strait transport is completely governed by the sea-surface difference because of the shallow depth. Third, the OBP data can be treated as a correction to the surface-layer transport for obtaining the total transport, particularly for the deep and narrow strait of Makassar and Luzon. Nevertheless, the theoretical estimation gives a consistent seasonal cycle and amplitude, much better than the method of using SSH or OBP alone, indicating that the combination of the two satellite data has the potential for estimating the transports through these straits.

[22] Lastly, we examine the residual transport after removing the mean and annual cycle. Figure 7 gives the comparison of the long-term residual transports with the Nino3.4 index (red). It can be seen that all the four residual transports have some correlation with the ENSO events, but the Karimata-Makassar and Luzon transports are more closely correlated with the Nino3.4 index. The ENSO correlation with the cross-strait flows in this region has been reported by *Qu et al.* [2004] for the Luzon Strait transport and *Susanto et al.* [2000] and *Qu et al.* [2005] for the Makassar Strait transport. Our model results are consistent with those previous studies. It should be noted that the agreement between the formula and model is not as good as the annual cycle case (not showing). This is not surprising because many other processes, besides the pressure gradient force, may also contribute to the transports between two interconnected oceans [*Burnett et al.*, 2003]. Such processes, including the non-linear dynamics, vertical and horizontal mixing, and deep water mass formation, cannot be predicted by the theoretical formulation.

5. Summary and Discussions

[23] In this study we have explored the possibility of using future satellite-derived OBP data to estimate interbasin transport. The proposed method is a combination of “geostrophic control” formula of *Garrett and Toulany* [1982] and the rotating hydraulics of *Whitehead et al.* [1974]. As satellite data are continuous in both space and time, it is essential for better use of data in obtaining interbasin transports that are fundamentally important to oceanography [*Whitehead*, 1998; *Godfrey*, 1996] and ocean climate considerations [*Dickson et al.*, 1999; *Hansen et al.*, 2001; *Gordon et al.*, 2003]. The new method appears to complement the traditional approach of using in-situ density profiles in two aspects: (1) Satellite-derived SSH and OBP provides spatial and temporal continuous data that can be used to estimate both long- and short-term variability of the transport. (2) Combining both surface and bottom data offers a natural way for separating the strait transport into surface and bottom fluxes that are important for characterizing the exchange of water mass. In addition, these satellite estimations complement the *in-situ* measurements [e.g., *Gordon et al.*, 2003] and provide necessary open-boundary conditions to regional ocean models [*Burnett et al.*, 2003]. As the new approach only needs area-averaged values of OBP and SSH near the strait, it is not particularly limited by satellite sampling resolution.

[24] As the first part of this study, we have focused on establishing the theoretical method (see Appendix A) and verifying the methodology by model-derived GRACE-proxy data. The verification, based on the Asian Marginal Seas with several interconnected straits and challenging complexity of coastal geometry, is quite promising. It is shown that the annual cycle of the strait transports is mainly controlled by the SSH and OBP gradients between two connected basins, and can be estimated effectively by using the satellite data. Finally, the residual transports of the Karimata-Makassar and Luzon straits are significantly correlated with ENSO events and would be difficult to be estimated by the simple theoretical formulation precisely. Our follow-up study will focus on testing in-situ measure-

ments and GRACE-derived OBP data. We also believe such a method has great potential for studying other sea straits of the world oceans.

Appendix A: Mathematical Derivation

[25] The mathematical derivation of formula (8) is a combination of the “geostrophic control” formula of *Garrett and Toulany* [1982] and the “hydraulic control” formulation of *Whitehead et al.* [1974]. We have used the former for the upper-layer flow and the latter for the lower-layer flow, as shown schematically in Figure 3.

A1. Geostrophic Control

[26] *Garrett and Toulany* [1982] have shown that the fluctuating barotropic flow through a strait is largely driven by the difference in sea level between two connected bodies of water. The model is based on the assumptions of a cross-strait geostrophic balance and an along-strait balance between the pressure gradient, acceleration and friction:

$$\begin{cases} vf = g\eta_x \\ \frac{\partial v}{\partial t} = -g\eta_y - \lambda v \end{cases} \quad (A1)$$

where v is the along-strait flow and λ is the bottom friction. For an idealized strait with a width W and length L and sea level locations, as shown in Figure A1a, they further assume that $\eta_4 = \eta_1$ and $\eta_5 = \eta_2$ to be consistent with Kelvin wave propagation in the two basins imposing values on η_4 and η_5 . The assumptions and $v = \text{Re}[Ve^{i\omega t}]$ lead to:

$$\begin{cases} Vf \frac{W}{L} = g \frac{\eta_3 - \eta_1}{L} \\ (i\omega + \lambda)V = -g \frac{\eta_3 - \eta_2}{L} \end{cases} \quad (A2)$$

Eliminating η_3 in above equations gives the along-strait flow:

$$V = \frac{g}{L}(\eta_2 - \eta_1) \left\{ i\omega + \lambda + f \frac{W}{L} \right\}^{-1}. \quad (A3)$$

It can be shown that for low-frequency changes of seasonal and annual scales ($\omega \sim 10^{-6}$), for reasonable estimates of the bottom friction coefficient ($\lambda = C_d U/H \approx 10^{-3} \times 0.5 \times 10^{-2} = 5 \times 10^{-6}$), and for straits that are not too long in relation to their width, the third term in (A3) tends to dominate, i.e., $\omega, \lambda \ll fW/L$ ($\sim 10^{-4}$). The volume flux in the upper layer then can be estimated by the formula:

$$Q_1 = \frac{g}{f} H_1 (\eta_2 - \eta_1) \equiv \frac{g}{f} H_1 \Delta\eta, \quad (A4)$$

where $\Delta\eta = \eta_2 - \eta_1$. The theoretical justification of the formulation has been further discussed by *Toulany and Garrett* [1984].

A2. Hydraulic Control

[27] *Whitehead et al.* [1974] has shown that rotating hydraulics can be used to oceanography for estimating strait

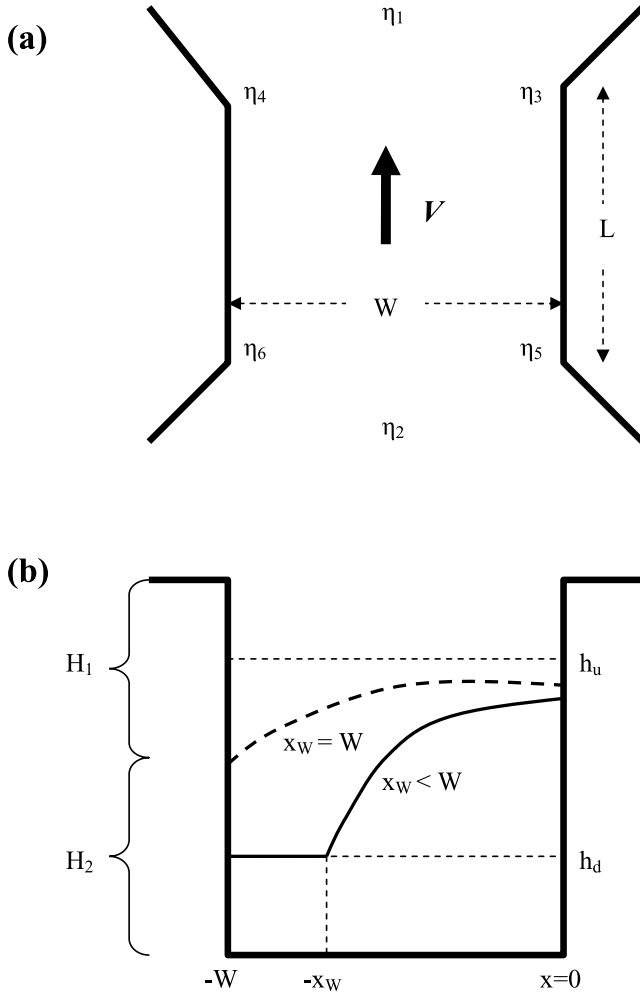


Figure A1. (a) Plan view of the sea levels associated with flow through the strait of length L and width W connecting two large water bodies. (b) Vertical view of the layer-interface for the case of $R < W$, in which $x_w < W$ (solid curve), and for the case of $R \geq W$, in which $x_w = W$ (dashed curve). Here h_u is the upstream height and h_d is the downstream height above the sill tip.

transports. Their formulation is initially based on the assumptions of geostrophic relation and zero potential:

$$\begin{cases} vf = g'h_x \\ v_x + f = 0 \end{cases} \quad (\text{A5})$$

and the constant Bernoulli and maximum transport (hydraulic control) condition:

$$\begin{cases} \frac{v^2}{2} + g'h = B(\psi) \\ \frac{\partial Q}{\partial h_0} \Big|_{\Delta h} = 0 \end{cases} \quad (\text{A6})$$

Here h is the profile of the layer-interface, h_0 is the value at $x = 0$, $B(\psi)$ is the Bernoulli of the stream function ψ , and Δh is the difference between the upstream height h_u and

downstream height h_d above the sill tip, as shown in Figure A1b. The above equations have solutions in two regimes. If the Rossby radius of deformation $R = \sqrt{2g'\Delta h}/f < W$, then $x_w = R$, and it can be shown that the solution and the strait transport Q_m within the layer $\Delta h = h_u - h_d$ have the following form:

$$\begin{cases} h = \Delta h - \frac{f^2 x^2}{2g'} \\ v = -fx \\ Q_m = \frac{g'\Delta h^2}{2f} \end{cases} \quad (\text{A7})$$

Otherwise, if $R \geq W$, then $x_w = W$, and the solution and the strait transport have the form:

$$\begin{cases} h = \frac{2}{3}\Delta h - \frac{f^2}{2g'} \left\{ x^2 + Wx + \frac{W^2}{6} \right\} + \frac{fG}{2\sqrt{3}g'} \left\{ x + \frac{W}{2} \right\} \\ v = -f \left\{ x + \frac{W}{2} \right\} + \frac{G}{2\sqrt{3}} \\ Q_m = \left(\frac{2}{3} \right)^{3/2} \frac{W}{8\sqrt{8}g'} \{ 8g'\Delta h - f^2 W^2 \}^{3/2} \end{cases} \quad (\text{A8})$$

Here $G = \sqrt{8g'\Delta h - W^2 f^2}$. If the downstream height h_d is above the sill tip, a case that was not considered by *Whitehead et al.* [1974], the overflow below h_d can be easily calculated by integrating the solutions as the following:

$$Q_d = \int_{-x_w}^0 h_d v dx = \begin{cases} \frac{g'}{f} h_d \Delta h & \text{if } R = \sqrt{2g'\Delta h}/f < W \\ \frac{G}{2\sqrt{3}} h_d W & \text{Otherwise} \end{cases} \quad (\text{A9})$$

The total volume transport in the strait is the sum of upper-layer transport Q_1 (geostrophic control volume) and lower-layer transport Q_m and Q_d (hydraulic control volume):

$$Q = \begin{cases} \frac{g'}{f} H_1 \Delta \eta + \frac{g'}{f} \left(\frac{\Delta h}{2} + h_d \right) \Delta h & \text{if } R = \sqrt{2g'\Delta h}/f < W \\ \frac{g'}{f} H_1 \Delta \eta + \left(\frac{2}{3} \right)^{3/2} \frac{W G^3}{8\sqrt{8}g'} + \frac{W h_d G}{2\sqrt{3}} & \text{Otherwise} \end{cases} \quad (\text{A10})$$

Since $2g'\Delta h \geq W^2 f^2 \geq 0$ in the second regime of the formulation, we approximate the cubic factor G^3 by the product of the upper limit of $G^2 = 8g'\Delta h - W^2 f^2 \approx 6g'\Delta h$ and the lower limit of $G = \sqrt{8g'\Delta h - W^2 f^2} \approx \sqrt{8g'\Delta h}$. The simplification yields:

$$Q = \begin{cases} \frac{g'}{f} H_1 \Delta \eta + \frac{g'}{f} \left(\frac{\Delta h}{2} + h_d \right) \Delta h & \text{if } R < W \\ \frac{g'}{f} H_1 \Delta \eta + \frac{W}{\sqrt{3}} \left(\frac{\Delta h}{2} + h_d \right) \sqrt{2g'\Delta h} & \text{Otherwise} \end{cases} \quad (\text{A11})$$

For computational simplicity, we further assume $\frac{\Delta h}{2} + h_d \approx \frac{1}{2}H_2$ in the case of $R < W$ and $\frac{2}{3}H_2$ otherwise, and then obtain the formulation:

$$Q = \begin{cases} \frac{g}{f} H_1 \Delta \eta + \frac{H_2}{2f} g' \Delta h & \text{if } R < W \\ \frac{g}{f} H_1 \Delta \eta + \left(\frac{2}{3}\right)^{3/2} H_2 W \sqrt{g' \Delta h} & \text{Otherwise} \end{cases} \quad (\text{A12})$$

It should be noted that Whitehead's hydraulic control theory has two major assumptions: the upper layer is motionless and the flow in the trait is relative slow. In fact, Whitehead's first assumption can be recovered by setting $\Delta \eta = 0$ (motionless upper layer) and $H_2 = \Delta h$ in the above equation. The second assumption is still valid for the seasonal and interannual timescales of flow in the strait because satellite-observed SSH and OBP are 10-day and monthly mean values.

[28] **Acknowledgments.** The research was carried out at the Jet Propulsion Laboratory, California Institute of Technology, under contract with the National Aeronautics and Space Administration (NASA). This work was also funded by the Office of Naval Research (N00014-03-IP-20059). Constructive comments from two reviewers are appreciated.

References

- Burnett, W. H., V. M. Kamenkovich, A. L. Gordon, and G. L. Mellor (2003), The Pacific/Indian Ocean pressure difference and its influence on the Indonesian Seas circulation: Part I—The study with specified total transports, *J. Mar. Res.*, *61*, 577–611.
- Chu, P. C., and R. Li (2000), South China Sea isopycnal-surface circulation, *J. Phys. Oceanogr.*, *30*, 2419–2438.
- Dickson, B., J. Meincke, I. Vassie, J. Jungclaus, and S. Osterhus (1999), Possible predictability in overflow from the Denmark Strait, *Nature*, *397*, 243–246.
- Drinkwater, M. R., R. Floberghagen, R. Haagmans, D. Muzi, and A. Popescu (2003), GOCE: ESA's first earth explorer core mission, in *Earth Gravity Field From Space: From Sensors to Earth Sciences*, *Space Sci. Rev. Ser.*, vol. 18, pp. 419–432, Springer, New York.
- Fang, G. H. (1995), The structure of the Taiwan-Tsushima-Tsugaru Current System and its relation to the Kuroshio (in Chinese with English abstract), *Mar. Sci.*, *4*, 43–48.
- Garrett, C. J. R., and B. Toulany (1982), Sea level variability due to meteorological forcing in the northeast of St. Lawrence, *J. Geophys. Res.*, *87*, 1968–1978.
- Godfrey, J. S. (1996), The effect of the Indonesian throughflow on ocean circulation and heat exchange with the atmosphere: A review, *J. Geophys. Res.*, *101*, 12,217–12,237.
- Gordon, A. L., and R. Fine (1996), Pathways of water between the Pacific and Indian Oceans in the Indonesian seas, *Nature*, *379*, 146–149.
- Gordon, A. L., R. D. Susanto, and K. Vranes (2003), Cool Indonesian Throughflow is a consequence of restricted surface layer flow, *Nature*, *425*, 824–828.
- Hansen, B., W. R. Turrell, and S. Osterhus (2001), Decreasing overflow from the North seas into the Atlantic Ocean through the Faroe Bank channel since 1950, *Nature*, *411*, 927–930.
- Hsueh, Y., J. R. Schults, and W. R. Holland (1997), The Kuroshio flow-through in the East China Sea: A numerical model, *Prog. Oceanogr.*, *39*, 79–108.
- Hu, J., H. Kawamura, H. Hong, and Y. Qi (2000), A review on the currents in the South China Sea: Seasonal circulation, South China Sea warm current and Korishio intrusion, *J. Oceanogr.*, *56*, 607–624.
- Huang, R. X., and X. Jin (2002), Sea surface elevation and bottom pressure anomalies due to thermohaline forcing, Part I: Isolated perturbations, *J. Phys. Oceanogr.*, *32*, 2131–2150.
- Hughes, C. W., and M. J. Smithson (1996), Bottom pressure correlations to the southern Atlantic, *Geophys. Res. Lett.*, *23*, 2243–2246.
- Hughes, C. W., C. Wunsch, and V. Zlotnicki (2000), Satellite peers through the oceans from space, *Eos Trans. AGU*, *81*(7), 68.
- Jayne, S. R., J. M. Wahr, and F. Bryan (2003), Observing ocean heat content using satellite gravity and altimetry, *J. Geophys. Res.*, *108*(C2), 3031, doi:10.1029/2002JC001619.
- Killworth, P. D. (1995), Hydraulic control and maximal flow in rotating stratified hydraulics, *Deep Sea Res.*, *42*, 859–871.
- Kim, Y., T. Takikawa, H. An, and J. Yoon (2004), The seasonal and inter-annual variability of the volume transport through the western channel of the Korea Strait, *J. Korea Soc. Oceanogr.*, *39*, 155–162.
- Li, L., W. D. Nowlin Jr., and J. L. Su (1998), Anticyclonic rings from the Kuroshio in the South China Sea, *Deep Sea Res.*, *45*, 1469–1482.
- Luther, D. S., A. D. Chave, J. H. Filloux, and P. F. Spain (1990), Evidence for local and nonlocal barotropic responses to atmospheric forcing during BEMPEX, *Geophys. Res. Lett.*, *17*(7), 949–952.
- Metzger, E. J., and H. E. Hurlburt (1996), Coupled dynamics of the South China Sea, the Sulu Sea, and the Pacific Ocean, *J. Geophys. Res.*, *101*, 12,331–12,352.
- Meyers, G., R. J. Bailey, and A. P. Worby (1995), Geostrophic transport of Indonesian Throughflow, *Deep Sea Res.*, *42*, 1163–1174.
- Pratt, L. J. (2004), Recent progress on understanding the effects of rotation in models of sea straits, *Deep Sea Res.*, *51*, 351–369.
- Qu, T., H. Mitsudera, and T. Yamagata (2000), Intrusion of the North Pacific waters into the South China Sea, *J. Geophys. Res.*, *105*, 6415–6424.
- Qu, T., Y. Y. Kim, M. Yaremchuk, T. Tozuka, A. Ishida, and T. Yamagata (2004), Can Luzon Strait transport play a role in conveying the impact of ENSO to the South China Sea?, *J. Clim.*, *17*, 3644–3657.
- Qu, T., Y. Du, G. Meyers, A. Ishida, and D. Wang (2005), Connecting the tropical Pacific with Indian Ocean through South China Sea, *Geophys. Res. Lett.*, *32*, L24609, doi:10.1029/2005GL024698.
- Qu, T., J. B. Girton, and J. A. Whitehead (2006), Deepwater overflow through Luzon Strait, *J. Geophys. Res.*, *111*, C01002, doi:10.1029/2005JC003139.
- Shaw, P.-T. (1991), The seasonal variation of the intrusion of Philippine Sea water into the South China Sea, *J. Geophys. Res.*, *96*, 821–827.
- Song, Y. T., and D. B. Haidvogel (1994), A semi-implicit ocean circulation model using a generalized topography-following coordinate, *J. Comput. Phys.*, *115*, 228–244.
- Song, Y. T., and T. Y. Hou (2006), Parametric vertical coordinate formulation for multi-scale, Boussinesq, and non-Boussinesq ocean modeling, *Ocean Modell.*, doi:10.1016/j.ocemod.2005.01.001.
- Song, Y. T., and T. Tang (2002), Eddy-resolving simulations for the Asian marginal seas and Kuroshio using the nonlinear-terrain following coordinate system, *J. Korean Oceanogr.*, *37*, 169–177.
- Song, Y. T., and V. Zlotnicki (2004), Ocean bottom pressure waves predicted in the tropical Pacific, *Geophys. Res. Lett.*, *31*, L05306, doi:10.1029/2003GL018980.
- Susanto, R. D., and A. L. Gordon (2005), Velocity and transport of the Makassar Strait throughflow, *J. Geophys. Res.*, *110*, C01005, doi:10.1029/2004JC002425.
- Susanto, R. D., A. L. Gordon, J. Sprintall, and B. Herunadi (2000), Intra-seasonal variability and tides in Makassar Strait, *Geophys. Res. Lett.*, *27*, 1499–1502.
- Tapley, B. D., S. Bettadpur, M. Watkins, and C. Reigber (2004), The Gravity Recovery and Climate Experiment: Mission overview and early results, *Geophys. Res. Lett.*, *31*, L09607, doi:10.1029/2004GL019920.
- Toulany, B., and C. J. R. Garrett (1984), Geostrophic control of fluctuating barotropic flow through straits, *J. Phys. Oceanogr.*, *14*, 649–655.
- Wahr, J., M. Molenaar, and F. Bryan (1998), Time variability of the Earth's gravity field: Hydrological and oceanic effects and their possible detection using GRACE, *J. Geophys. Res.*, *103*, 30,205–30,229.
- Wahr, J., S. Sweson, V. Zlotnicki, and I. Velicogna (2004), Time-variable gravity from GRACE: First results, *Geophys. Res. Lett.*, *31*, L11501, doi:10.1029/2004GL019779.
- Wajsovicz, R. C. (1993), A simple model of the Indonesian Throughflow and its composition, *J. Phys. Oceanogr.*, *23*, 2683–2703.
- Whitehead, J. A. (1989), Internal hydraulic control in rotating fluids—applications to oceans, *Geophys. Astrophys. Fluid Dyn.*, *76*, 1–27.
- Whitehead, J. A. (1998), Topographic control of oceanic flows in deep passages and traits, *Rev. Geophys.*, *36*, 423–440.
- Whitehead, J. A., A. Leetmaa, and R. A. Knox (1974), Rotating hydraulics of strait and sill flows, *Geophys. Fluid Dyn.*, *6*, 101–125.
- Wyrtki, K. (1961), Physical oceanography of the Southeast Asian waters, vol. 2, NAGA report, 195 pp., Univ. of Calif., San Diego.
- Wyrtki, K. (1987), Indonesian through flow and the associated pressure gradient, *J. Geophys. Res.*, *92*, 12,942–12,946.
- Zlotnicki, V., J. Wahr, I. Fukumori, and Y. T. Song (2006), The Antarctic Circumpolar Current: seasonal transport variability during 2002–2005, *J. Phys. Oceanogr.*, in press.

Y. T. Song, Jet Propulsion Laboratory, California Institute of Technology, 4800 Oak Grove Drive, Pasadena, CA 91009, USA. (song@pacific.jpl.nasa.gov)